Membrane Cholesterol-Dependent Dual VEGFR2/FGFR1 Inhibition by Ginsenoside Rg3 to Overcome Gefitinib Resistance in NSCLC

Min Jiang*[a], Chao Hong*[# a,b], Wenkui Zou*[a], Zheng Ye[a], Kexu Gu[a], Yaning Ren[a], MingFang Li[a], Don Green[c], Tong Zhang[#a,b], Yue Ding[#a,b,d]

[a] School of Pharmacy, Shanghai University of Traditional Chinese Medicine, Shanghai, 201203, Republic of China;

[b] State Key Laboratory of Integration and Innovation of Classic Formula and Modern Chinese Medicine, Shanghai University of Traditional Chinese Medicine, Shanghai 201203, China;

[c]School of Human Sciences, London Metropolitan University, London N7 8DB, Britain;

[d] National Innovation Platform for medical industry-education integration, Shanghai University of Traditional Chinese Medicine, Shanghai 201203, China;

[#] Corresponding authors: dingyue-2001@hotmail.com, Tel: 021-51322332; zhangtongshutcm@hotmail.com, Tel:021-51322318; shutcmhong@163.com, Tel:021-51322325

* These authors contributed equally to this work.

Abstract

Background: Drug resistance severely hinders the clinical application of epidermal growth factor receptor tyrosine kinase inhibitors (EGFR-TKIs) in the treatment of non-small cell lung cancer (NSCLC). Notably, resistance caused by rare target mutations (with a mutation incidence rate below 5%) accounts for approximately 15% of total resistance cases in NSCLC. Due to the diversity and complexity of these mutations, targeted therapies against them are currently very limited.

Purpose: To address the challenge of multi-driver resistance in NSCLC, this study aimed to explore a novel therapeutic strategy that can simultaneously inhibit multiple resistance drivers and enhance drug resensitization to EGFR-TKIs, overcoming the limitations of conventional single-protein inhibitors.

Methods: Established gefitinib-resistant HCC827 cell models driven by rare co-activation of two EGFR-independent membrane proteins. Developed a strategy targeting lipid raft cholesterol to destabilize raft integrity, leveraging the cholesterol-modulating properties of ginsenosides. Evaluated the synergistic effect of co-administering ginsenoside Rg3 with gefitinib in both in vitro and in vivo models. Explored the mechanism of Rg3 action, including its binding to lipid raft cholesterol, disruption of membrane anchoring of resistance-associated receptor tyrosine kinases, and acceleration of their endocytic degradation.

Results: Co-administration of ginsenoside Rg3 with gefitinib synergistically restored antitumor efficacy in both in vitro and in vivo models, outperforming conventional single-protein inhibitors. Mechanistically, Rg3 specifically binds to lipid raft cholesterol, disrupting the membrane anchoring of resistance-associated receptor tyrosine kinases (e.g., FGFR1 and VEGFR2) and accelerating their endocytic degradation. Structural-activity relationship analyses revealed that the cholesterol-binding capacity of ginsenosides—critical for resistance reversal—is modulated by the stereochemical configuration of sugar moieties at C3, C6, and C20 positions.

Conclusions: This study elucidates a novel membrane-centric paradigm for overcoming multi-driver resistance in NSCLC, where pharmacological perturbation of cholesterol-lipid raft interactions by natural compounds like Rg3 enables broad-spectrum suppression of coexisting resistance mechanisms. It not only provides novel insights into the mechanisms underlying resistance in NSCLC but also presents a promising clinical strategy that could significantly improve treatment outcomes for patients.

Keywords:

Rare co-mutation, gefitinib-resistance, lipid rafts cholesterol, ginsenosides

Abbreviations

Chol, cholesterol; CAV-1, caveolin-1;EGFR-TKI, growth factor receptor tyrosine kinase inhibitor; FGFR1, fibroblast Growth Factor Receptor 1; GFB, Gefitinib; GCS, glycyrrhizic acid; GP, generalized polarization; LUVs, large unilamellar vesicles; Mβ CD, methyl-β-cyclodextrin; NSCLC, non-small cell lung cancer; Rg3, ginsenoside Rg3;

VEGFR2, vascular endothelial growth factor receptor 2.

Introduction

Non-small cell lung cancer (NSCLC), the most prevalent form of lung cancer, is characterized by aggressive behavior and poor prognosis(Clark and Alsubait, 2024; Ganti et al., 2021) . Treatment outcomes have been significantly improved since the beginning of this century, primarily due to the development and introduction of EGFR-TKIs. EGFR-TKIs provide a promising treatment outcome in EGFR mutation-positive patients, who achieved a response rate as high as 80% and approximately 10-14 months of progression-free survival (PFS)(Wu and Shih, 2018). Unfortunately, long-term treatment with EGFR TKIs often leads to acquired resistance within 9-12 months, thereby limiting its overall therapeutic benefit. The most common resistance mechanism associated with the first and second generation TKIs like gefitinib is the development of EGFR T790M mutation (~50% frequency)(Denis et al., 2015; Westover et al., 2018). Third-generation EGFR-TKIs, represented by Osimertinib, have significantly improved the drug resistance problem of first- and second-generation drugs by targeting the EGFR T790M mutation(Soria et al., 2018). However, for "off-target resistance", that is, drug resistance caused by by-pass activation due to other gene abnormalities. In addition to MET amplification (15-20%), HER2 amplification (12-15%), and RET fusion (5-10%) (Husain et al., 2017) mutation patients who can be treated with precise combination therapy targeting the mutation sites by combining MET inhibitors (such as Capmatinib) or antibody-drug conjugates like T-DXd (Enhertu). And rare targets with tumor driver gene mutation rate of less than 5%, such as ROS1 rearrangement, BRAF mutation, FGFR1-TACC1 fusion, and VEGFR activation, still lack effective clinical treatment drugs and can only be treated conservatively with chemotherapy (Cho et al., 2023; Liu et al., 2018; Liu et al., 2021). These orphan targets have long lacked effective drugs due to the complexity of their molecular mechanisms, the existence of multiple independent clones of membrane proteins that by-pass and activate the targets. And the compensatory enhancement of other pathways after the inhibition of one pathway, making it difficult for single-target drugs to block the signaling network(Wang et al., 2023). However, rare mutations account for a large proportion overall, with a total of about 15% of all lung cancers(Riely et al., 2024).This can be construed as approximately one out of every

seven lung cancer patients having a mutation in a rare target as the reason for drug resistance. Therefore, rare mutations in lung cancer need to be given significant attention, and there is an urgent need to further explore effective treatment methods for NSCLC drug resistance caused by rare mutations.

Reprogramming of cholesterol synthesis and metabolism is a hallmark of cancers(Huang et al., 2020; Kuzu et al., 2016). Besides serving as a component of the cell membrane, cholesterol is extensively found in lipid rafts, which are small regions within the membrane that function as platforms for cellular signaling processes(Isik and Cizmecioglu, 2023). The unique ability of lipid rafts to selectively include or exclude proteins makes lipid rafts significant contributors to tumor progression and the development of drug resistance(Wu et al., 2022; Zhang et al., 2024). Notably, several key proteins associated with drug resistance, including receptor tyrosine kinases and ATP-binding cassette (ABC) transporters, exhibit a reversible association with lipid rafts in response to specific signals(Gupta et al., 2018; Ruzzi et al., 2024). This observation leads us to hypothesize that by destabilizing the lipid rafts this may simultaneously impair the function of multiple co-mutated bypass proteins, which are implicated in gefitinib resistance in NSCLC. To accomplish this, targeting cholesterol, a crucial component of lipid rafts for maintaining their structure and function, becomes essential. Previous studies have demonstrated that cholesterol depletion disrupts lipid rafts, causing substantial alterations in cellular functions(Gu et al., 2024; Lv et al., 2021). Therefore, building upon these foundations, we propose a novel therapeutic paradigm: Precision modulation of raft cholesterol content may achieve concurrent suppression of coexisting resistance drivers, thereby overcoming the current limitations of single-pathway targeting in NSCLC with polyclonal resistance mutations. This membrane-centric strategy holds promise for reversing multidrug resistance patterns arising from heterogeneous genomic alterations.

Ginsenosides, the primary pharmacologically active components of ginseng, exhibit structural similarity to cholesterol, and their effects are largely attributed to their ability to interact with plasma membrane cholesterol, thereby influencing cellular functions such as cell survival(Arabi et al., 2024; Garza-Miyazato et al., 2024). Multiple studies have shown that ginsenosides can disrupt cholesterol-lipid rafts, leading to anti-proliferative and pro-apoptotic effects in different types of cancer cells(Kwon et al., 2008; Qiu et al., 2022; Yun et al., 2013). ginsenoside Rh2 has been shown to induce

apoptosis by disrupting lipid rafts through the oligomerization of the FAS death receptor in HeLa cells, or by inactivating Akt via a serine/threonine kinase in human epidermoid carcinoma A431 and breast cancer MDA cells(Park et al., 2010). Furthermore, Rh2 can mitigate Alzheimer's disease symptoms that can be alleviated by promoting the non-amyloidogenic processing of the amyloid precursor protein (APP) through a pathway dependent on cholesterol and lipid rafts(Qiu et al., 2014). In another study, treatment with 20S-protopanaxadiol was found to reduce Akt activity in the lipid rafts of the glioma cell line U87 MG, while it increased Akt activity in neuroblastoma N2a cells, due to the regulation of raft-associated dephosphorylation(Liu et al., 2011). Given its chemical structure resembling that of cholesterol, it is plausible that this ginsenoside may intercalate into lipid rafts, resulting in alterations within the membrane microenvironment(Kwon et al., 2008). Thus, based on the close correlation among cholesterol-lipid raft-membrane protein, we postulate that by targeting lipid raft cholesterol via ginsenoside this would simultaneously regulate multiple drug-resistance-associated proteins on the membrane, which holds promise for addressing EGFR-TKI resistance characterized by multiple protein co-mutations. This study seeks to establish a model of NSCLC marked by the abnormal co-expression of various by-pass proteins, culminating in gefitinib resistance. Subsequent efforts involved the screening and reversal of acquired drug resistance through ginsenoside intervention, alongside an in-depth exploration and validation of the associated regulatory pathways involving membrane cholesterol-lipid raft interactions and multimembrane proteins. Furthermore, to validate the generality of this therapeutic strategy, we also established breast cancer cells resistant to chemotherapeutic drugs, and demonstrated that ABC transporters can similarly be inhibited through targeted regulation of lipid raft cholesterol by Rg3, thereby reversing their drug resistance.

Materials and Methods

Reagents

Gefitinib, Ginsenoside Rg3 and other ginsenoside saponins, paclitaxel, digitonin and glycoside were purchased from Shanghai Yuanye Biotechnology (Shanghai, China). PD166866, Axitinib and Verapamil were purchased MedChemExpress (New Jersey, USA). MβCD were obtained from Aladdin (Shanghai, China). CCK-8 assay was bought

from Beyotime Biotechnology (China). Filipin III kit was brought from the Abcam (USA). TopFluor® cholesterol was obtained from the Sigma-Aldrich (USA). Laudran was obtained from the MedChemExpress (New Jersey, USA).

Cell culture

Human cell lines HCC827 were purchased from National Collection of Authenticated Cell Cultures (China). The cells were cultured in RMPI-1640 with 10% FBS, glutamine and 1% penicillin streptomycin (Gibco) at 37 °C and 5% CO_2. To establish gefitinib-resistant cell lines (GR), HCC827 cells were cultured with increasing doses of gefitinib starting from 5nM. Drug-containing medium was added after cell adhesion growth for 24 h, and passaged when the cell spread across 90%. After the replication of the passage cell, the concentration was increased by 10nM until HCC827 cells could proliferate quickly in the presence of 1μM gefitinib. This induction process takes at least 6-7 months. The resistant cell lines were named HCC827/GR. HCC827 and HCC827/GR cells were authenticated by STR profiling and flow cytometry.

Mouse model

The sensitive cell line HCC827 and the drug-resistant cell line HCC827/GR were subcutaneously injected into the right forelimb axilla of female BALB/c nude mice (4 weeks old). The cell densities were 2×10^6 cells per mouse for HCC827 and 5×10^6 cells per mouse for HCC827/GR, respectively. Once the tumor volume reached approximately 50-100 mm^3, the administration of the medication began. All mice were obtained from Shanghai Sippr-Bk Lab Animal Co., Ltd. (China) and maintained in a controlled environment (temperature 21°C ±1°C, humidity 55% ± 10%) with *ad libitum* access to food and water and a standard light-dark cycle. All experimental operations complied with the guidelines of the Institutional Animal Experimental Ethics Committee of SHUTCM (license file no. PZSHUTCM2306280002).

Cell cytotoxicity assay

Cell viability was determined by CCK-8 assay. Cells were treated with indicated drugs followed by adding 100uL CCK-8 solution per wells at 37°C for 4 h. Finally, the OD values of each well was measured using a microplate reader. The cell viability and IC_{50} were calculated using SPSS.

Western blot

To assess protein expression in cells or tumor tissues, proteins were extracted and equal amounts were separated using 10-15% SDS-PAGE. The proteins were then transferred to polyvinylidene difluoride (PVDF) membranes and blocked with Quick Block™ Blocking Buffer. The membranes were subsequently incubated overnight at 4°C with the following primary antibodies: anti-ABCB1, anti-CAV-1 (Cell Signaling Technology, Boston, MA, USA), anti-p-EGFR, anti-EGFR, anti-FGFR1, and anti-VEGFR2, anti-p-AKT, anti-AKT, anti-p-PI3K, anti-PI3K (Abcam, USA), anti-p-ERK, anti-ERK, anti-p-STAT3, anti-STAT3, anti-c-MET, anti-HER2, anti-HER3, anti-AXL, anti-β-ACTIN (Beyotime Biotechnology, Shanghai, China). Following this, the membranes were incubated with secondary antibodies (goat anti-mouse and goat anti-rabbit antibody-antigen complexes) at room temperature for 2h and then visualized using an ECL Western blotting detection system. The Western blot images were captured and analyzed with a Bio-Rad® Chemiluminescence Imaging System.

Immunofluorescent Staining

For colocalization studies, cells were grown in microscopy dishes. Following this, they were washed three times with PBS and stabilized with 4% paraformaldehyde for 20 minutes. After fixation, the cells underwent treatment with 0.05% Triton X-100 in PBS for 5 minutes to improve membrane permeability, and were then incubated with 2% BSA in PBS for 30 minutes to minimize non-specific binding. Subsequently, the cells were incubated overnight at 4°C with primary antibodies directed against ABCB1, FGFR1, VEGFR2 (1:500) (Abcam, USA), and CAV-1 (1:500) (Cell Signaling Technology, USA). After PBS washes, the cells were incubated with Alexa Fluor 488-conjugated Goat Anti-Rabbit IgG(H+L) and Alexa Fluor 647-conjugated Goat Anti-Mouse IgG(H+L) (Beyotime, China) for 1 hour at room temperature. This was followed by a 10-minute incubation with DAPI. Fluorescence imaging was performed using a confocal laser scanning microscope (CLSM, Leica TCS SP8).

Extraction and isolation of lipid rafts(Gajate and Mollinedo, 2021; Rabani et al., 2016)

Parental and drug-resistant cells in the logarithmic growth phase were harvested and

inoculated in 10-cm culture dishes. Once the cell density reached 70%-80% (approximately 5×10^7cells), the cells were collected, washed three times with cold PBS at 4°C, and placed on ice. Subsequently, 1 mL of lysis buffer was added while maintaining the sample on ice for a duration of 30 minutes. Following lysis, samples were centrifuged at 12,000 rpm/min at 4°C for 10 min to collect the supernatant. To this supernatant, an additional 1 ml of an 80% sucrose solution was added and mixed thoroughly by vortexing before transferring it to a 5 mL ultracentrifuge tube. Gradually added sequentially: first, 2mL of a 30% sucrose solution followed by adding 1 mL of a 5% sucrose solution to create distinct layers within the tube. The mixture was then subjected to ultracentrifugation at 4°C at 200,000g for 20h. Upon completion of centrifugation, carefully removed the centrifuge tube and extracted 400μL from each of the top 12 fractions formed in the sucrose gradient; these should be properly labeled and reserved for subsequent experiments. Additionally, in each fraction added 5×SDS loading buffer to prepare the protein samples. For localization analysis of lipid rafts, the marker proteins were utilized in immunoblotting assays, and total cholesterol content in extracted lipid raft samples were quantified using a total cholesterol assay kit.

Filipin III assays detect cell-membrane cholesterol content

The free cell-membrane cholesterol in HCC827 and HCC827/GR were stained with Filipin III and evaluated by means of CLSM. Cells were inoculated in confocal dishes and incubated for 24h. Subsequently, certain concentrations of ginsenosides were administered, and after 24h of incubation, the drugs were removed and the products of the Filipin III assay were incubated for staining. Then, the changes in fluorescence intensity were observed under CLSM.

LC/MS detect the total cholesterol content of the cells.

Parental HCC827 and drug-resistant HCC827/GR cells were acquired and placed in EP tubes. 1mL of lysis buffer composed of chloroform: isopropanol (7:11) was added. Ultrasonic treatment was implemented at 200w for 30min in each instance. 800μL of anhydrous methanol was introduced and vortexed for 5min to facilitate protein

precipitation. After a 5min standing duration, centrifugation was executed at 4℃ and 13000g for 10min. Once centrifugation had finished, the supernatant was retrieved and subjected to nitrogen blow drying at 50℃ (approximately 10-20min), followed by the addition of 200μL of deuterated cholesterol solution (100ng/mL) as an internal standard. After blow drying, 1mL of anhydrous methanol: water (9:1) was incorporated for reconstitution. Ultimately, the reconstituted solution was centrifuged at 4℃ and 13000g for 10min. The supernatant was collected and introduced into the mass spectrometer for detection.

Preparation of LUVs

Large unilamellar vesicles (LUVs) were fabricated via the thin film evaporation method using a formulation of DSPC: Cholesterol (Chol) at a molar ratio of 80:20. First, the two substances were dissolved in chloroform. Subsequently, a rotary evaporator was utilized to evaporate the solvents at 60°C (using a water bath) to create a thin film. Following this, the film was hydrated in a 250 mmol/mL ammonium sulfate solution at 60°C for 30min to produce a liposomal suspension. This suspension was then subjected to sonication using a SCIENTZ-IID ultrasonic processor (manufactured by Ningbo Scientz Biotechnology Co., Ltd., China) while being cooled in an ice bath to form large unilamellar vesicles (LUVs). The final liposomes were prepared via dialysis, and their particle size and zeta potential were measured. Lastly, the LUVs were kept at 4°C for storage.

TopFluor® cholesterol fluorescence spectroscopy in solution(Malabed et al., 2017)

TopFluor® cholesterol is a compound with the same properties as cholesterol, attached to a fluorophobe. The binding experiment with saponin was carried out using fluorescent cholesterol in place of cholesterol for examination, and fluorescence characterization was performed. Respectively, different concentrations of the stock solution of saponins were added to the TopFluor® cholesterol solution (1μg/mL), which contained 10 mM PBS (pH 7.4) and 0.1% DMSO, and incubated at room temperature

for 3h. Fluorescent enzyme marker was used for detection of the fluorescence of the combination solution. The fluorescence intensity characterized the binding ability of saponins to cholesterol.

Morphology of cell membrane in transmission electron microscope(Laurens et al., 1994)

Initially, cells were cultured at a density of 4×10^5 cells per dish and exposed to different concentrations of ginsenoside. The cells were then fixed with 1.5% glutaraldehyde in 0.1M sodium cacodylate buffer for 2h at 4°C. After three washes with sodium cacodylate buffer, the cells were post-fixed with 1% osmium tetroxide in 0.1M sodium cacodylate buffer for 1h and washed twice more with the buffer. Dehydration was carried out using a graded series of ethanol (30-100%) and 100% propylene oxide. The cells were infiltrated and embedded in Agar-100 resin, which was polymerized by heating overnight at 60°C. Ultrathin sections were prepared, and images were obtained using a Jeol JEM-1230 transmission electron microscope.

Laurdan stains cell membranes and characterizes the phase of the cell membrane(Lorent et al., 2016)

Following incubation, the cells were washed with culture media and labeled with 2μM Laurdan at 37°C for 30min in RPMI media containing 1mg/mL BSA. Fluorescence images were captured using a confocal laser scanning microscope (CLSM, Leica TCS SP8). Emission intensities were measured in two channels (I1=404–457nm and I2= 468–528 nm) across the entire cell. The generalized polarization (GP) was calculated using the formula: GP = (I1−G.I2) / (I1+G.I2). Ultraviolet spectrophotometry was used to detect the change in the membrane GP value after Laurdan staining.

***In vivo* antitumor effect**

According to the above tumor-bearing mouse model, we administered the drug to carry out *in vivo* pharmacodynamics experiments. After 1 week injection, in HCC827/GR cells, mice were randomly divided into six groups (n=6) based on tumor volume as follows: Control, gefitinib group (treated with 5mg/kg gefitinib), ginsenoside Rg3

group (treated with 40mg/kg ginsenoside Rg3), gefitinib+Rg3 group (treated with 5 mg/kg gefitinib and 40mg/kg ginsenoside Rg3) and inhibitors+gefitinib (treated with 1 mg/kg PD166866, 1mg/kg axitinib respectively and 5mg/kg gefitinib groups. In all experiments, gefitinib, PD166866 and axitinib were administrated by oral injection, while Rg3 was administrated by intraperitoneal injection.

Statistical analysis

Data analysis was performed using GraphPad Prism 9.0. T-tests or one-way ANOVA were employed to compare the data. Results are presented as mean ± SD. Statistical significance was set at $p < 0.05$, and the symbols are detailed in the figure legends. Because this was a pilot study, a formal power calculation was not required.

Results

Generation of cell models with acquired drug-resistant cells

To establish gefitinib-resistant NSCLC cell model, we gradually exposed the parent HCC827 cells to half of the IC_{50} concentrations of gefitinib over a period of six months (Figure 1A). The cells model was deemed established when HCC827 could proliferate freely in 1 μM gefitinib. We employed the CCK-8 assay to compare the drug resistance coefficients between the parental strain and the drug-resistant cells (Figure 1C, D). Notably, HCC827/GR exhibited significantly poorer responses to gefitinib compared to parental cells, with IC_{50} values being over 100 times greater than those of the parental strain (Figure 1E). To further validate their stability *in vivo*, we constructed a xenograft nude mouse tumor model to confirm the successful establishment of the drug-resistant cell line (Figure 1B). The results indicated that in the parental HCC827 cells, both high-dose and low-dose gefitinib can significantly inhibit the occurrence and development of tumors, and the tumor inhibition rate could reach 90% (Figure 1F-H). However, there was no discernible effect on tumor growth (Figure 1I-K) in the HCC827/GR cells, indicating that the *in vivo* tumor model of gefitinib resistance had been successfully constructed. And as the concentration increased, the toxicity also increased, so we conducted further experiments based on the low concentrations. Collectively, these drug-resistant models serve as valuable tools for elucidating molecular mechanisms that will be evaluated in subsequent experiments.

Activation of Dual Membrane Proteins Leading to Gefitinib Resistance in a cholesterol enriched lipid raft–dependent manner

To explore the mechanisms underlying acquired resistance to gefitinib in HCC827, we initially detected the expression of p-EGFR via Western Blot (Figure 2A). The results indicated that there was no abnormal overexpression of p-EGFR, suggesting that its resistance mechanism was not associated with the secondary mutation of EGFR. Meanwhile, the proteome analyses result (Figure S1a) showed that RTK family members increased dramatically in HCC827/GR cells, suggesting EGFR-independent activation of by-pass RTK proteins may serve as the inducement of gefitinib resistance. To validate this hypothesis, six most commonly occurring mutation by-pass proteins associated with gefitinib resistance were compared in HCC827 and HCC827/GR cells (Figure 2B). The results showed that, compared with the parental HCC827 cells, two of the membrane proteins, FGFR1 and VEGFR2, were abnormally upregulated in HCC827/GR cells, while the others were consistent with the parental expression, suggesting that FGFR1 and VEGFR2 are related to the occurrence of drug resistance. Therefore, we selected inhibitors corresponding to VEGFR2 (axitinib) and FGFR1 (PD166866) to further explore their roles in the gefitinib resistance model (Figure 2C). The results of the CCK-8 assay revealed that a single inhibitor could not reverse the resistance to gefitinib; however, the combined application of the two inhibitors could effectively reverse the situation, but it would cause relatively higher toxicity.

Then to further elucidate the mechanism of gefitinib resistance, the activation of three classical downstream signaling pathways of EGFR (RAS–RAF–MEK–ERK, JAK–STAT, and PI3K–AKT) was assessed (Figure 2D). Western blot analysis revealed a significant increase in p-AKT expression, whereas no notable changes were observed in p-ERK and p-STAT3, suggesting that the PI3K-AKT-mTOR signaling pathway maybe activated for the survival of HCC827 cells in the presence of gefitinib. To confirm this, we likewise employed the VEGFR2 and FGFR1 inhibitors to explore their inhibitory actions on downstream signaling pathways (Figure 2E). Single inhibitor hardly blocked the activation of AKT-mTOR pathway while combination of two inhibitors fully suppressed this classical pathway for cancer survival. Therefore, the aberrant co-overexpression of FGFR1/VEGFR2 proteins that mediates PI3K-AKT-mTOR activation is responsible for the gefitinib resistance in HCC827 cell (Figure 2F). Importantly, it is essential to simultaneously inhibit both membrane proteins to prevent

the development of resistance.

Drug-resistant associated membrane proteins were co-activated in a cholesterol enriched lipid raft–dependent manner

Lipid rafts are dynamic nanoscale assemblies of sphingolipids, cholesterol, and proteins that can stabilize and coalesce to form platforms involved in membrane signaling and trafficking. Many proteins are known to have functions that are closely associated with lipid raft domains on the cell membrane (Figure S1c, d). To investigate the interaction between the resistant membrane protein and the lipid raft, the colocalization of FGFR1 and VEGFR2 with lipid raft (marked as CAV-1) were clearly observed by confocal images (Figure 3A). Compared with the parental HCC827 cells, the expression of the lipid raft protein CAV-1 is anomalously elevated in the drug-resistant HCC827/GR cells (Figure 3B). Considering that cholesterol, a key component of lipid rafts, is essential for the stability of lipid rafts and the anchoring of proteins within them. Previous studies(Pan et al., 2022) have found that total cholesterol in gefitinib-resistant NSCLC cells was significantly higher than that in sensitive cells, however, the role of lipid raft cholesterol in gefitinib resistance occurring have not been fully understood. Here, Filipin III staining (Figure 3C) by CLSM observation also showed that the increased cholesterol content was mainly concentrated in the membrane region. We further detected the cholesterol level differences between the resistant and parental cells using LC-MS/MS (Figure 3D), and the total cholesterol content in HCC827/GR cells was significantly higher than that in the parental HCC827 cells.

Next, we isolated the lipid rafts in the cell membrane by density gradient centrifugation and determined the contents of cholesterol and resistant protein in the lipid rafts respectively. The results indicated that compared with HCC827 cells, the cholesterol content in lipid rafts increased significantly while no difference was found for free cholesterol (Figure 3E). Then, we conducted further measurement of cholesterol and two resistant related proteins at specific layers of lipid rafts to ascertain if there was a correlation between them (Figure 3F-I). In HCC827 cells, lipid rafts are predominantly distributed in layers 8 to 10, where the cholesterol accumulated mostly and resistant protein is mainly pronounced, a finding which corresponded to a previous report that cholesterol-enriched lipid raft could work as a platform for functional proteins(Lucero and Robbins, 2004). Interestingly, in the gefitinib-resistant HCC827

cells, the density distribution of lipid rafts is much wider (layers 7 to 12), indicating that the diversity of the lipid raft region had increased. However, drug-resistance proteins were still concentrated in the lipid raft layers (layers 10 to 12) where cholesterol was mostly abundant. Above all, small rafts can sometimes be stabilized to form larger platforms through protein-protein and protein lipid interactions(Pike, 2006). Once HCC827 acquired resistance, the cholesterol content in the cell membrane rose, leading to the expansion of the lipid raft domain's width and making the functional domain of lipid rafts more active in the expression of drug-resistant-related proteins. The activation of dual membrane proteins leading to gefitinib resistance probably occurred in a cholesterol enriched lipid raft-dependent manner, making raft-cholesterol a potential target for overcoming drug resistance (Figure 3J).

It has been also reported that the resistance of the chemotherapy drug paclitaxel is directly associated with the abnormally elevated cholesterol in lipid rafts and ABCB1(Fenyvesi et al., 2008). To validate our hypothesis, we constructed a cell line of MCF-7 with resistance to paclitaxel (PTX) (Figure S2), which is well-recognized for its drug resistance resulting from high expression of the membrane protein ABCB1(Figure S3). Additionally, studies have also reported a close correlation between its drug resistance and cellular cholesterol levels. In MCF-7/PTX cells, the efflux-related drug-resistant protein ABCB1 and the lipid raft protein CAV-1 are both highly expressed and co-localized well in the lipid raft area. As a consequence, cell membrane lipid rafts were also isolated by density gradient centrifugation (Figure S4). The results showed that ABCB1 protein is primarily localized within lipid raft domains, which were the most enriched in cholesterol, suggesting that the exertion of its efflux effect is likely to be closely related to the function of cholesterol-enriched lipid rafts. It is further demonstrated that the close correlation between this drug resistance protein and the cholesterol content in lipid rafts is of some specific significance. The modulation of cholesterol content in the lipid raft region to improve the drug resistance effect serves as an effective therapeutic target.

Ginsenoside Rg3 binds with membrane cholesterol to reverse gefitinib resistance

Ginsenosides are widely reported to have good affinity for cholesterols. Therefore, we selected a total of 14 commercially available ginsenosides and screened them for

their ability to reverse drug resistance (Figure S5). Cytotoxic testing clearly showed that ginsenoside Rg3 exhibited a favorable reversal of drug resistance effect in both cell lines (Figure 4A), and its reversal enhancement of drug resistance for gefitinib was 4.3-fold. We further explored the correlation between the reversal of drug resistance and the role played by cholesterol in this behavior. In the drug-resistant cell lines HCC827/GR (Figure 4B), the reversal effect of drug resistance by ginsenoside Rg3 was comparable to that of the positive drug MβCD. Nevertheless, the reversal effects of drug resistance by ginsenoside Rg3 were significantly inhibited after the addition of free cholesterol, indicating that the effect of ginsenoside Rg3 is closely related to the interaction with cholesterol. We employed the total cholesterol (T-CHO) kit to study the impact of ginsenoside Rg3 on the cholesterol levels in the two drug-resistant cell lines (Figure 4C). The results presented showed that Rg3 can effectively reduce the total cholesterol content in both HCC827/GR cells, and its efficacy is comparable to that of the positive control lovastatin (Lova), a targeted inhibitor of cholesterol biosynthesis.

As reported elsewhere, nearly 80% of cholesterol is distributed in cell membranes. Next, we utilized the Filipin III assay to detect the changes of cholesterol in the cell membrane after treatment with ginsenoside Rg3 (Figure 4D). As the results depicted, ginsenoside Rg3 can markedly reduce the cell membrane fluorescence intensity in both cells, suggesting that it can down-regulate the cholesterol content in the cell membrane. The Laurdan reagent is a sensitive membrane fluorescence probe, which can combine with the lipid composition of the membrane to characterize the fluidity and phase transitions of the cell membrane(Lorent et al., 2016). The cholesterol remover MβCD was used as a positive control here (Figure 4E, F). Under the effect of ginsenoside Rg3, the fluorescence intensity significantly decreased, comparable to that of the positive drug MβCD, which implied that Rg3 can reduce the lipid content of the cell membrane. After treatment with ginsenoside Rg3, the pseudopodia of the cell membrane were significantly inhibited, and the originally irregular surface antenna shape became round and smooth, thereby reducing the migratory capacity of the drug-resistant cells. Nevertheless, this effect can be restored by additional cholesterol supplementation. The GP value of the cell membrane was calculated using a fluorescence spectrophotometer. The results showed that the GP value of the cell membrane rose after the treatment of Rg3, suggesting that the cell membrane rearranged from the original fluid state to the

gel state. Meanwhile, the effect of ginsenoside Rg3 on cell membrane morphology was observed under transmission electron microscope (Figure 4G). In the control group, the surface membrane appeared exceptionally smooth, characterized by numerous microvilli on the outer layer. Following the addition of ginsenoside Rg3 at varying concentrations, the membrane surface became irregular, with membrane fractures occurring to differing extents as the concentration increased. As indicated by the red arrow, microvilli detached from the surface, revealing specialized structures external to the membrane (these specialized structures comprised lipid components within the cell membrane, including phospholipids and cholesterol). The results suggested that drug-resistant cell membranes can be disrupted under ginsenoside Rg3 treatment. It was further demonstrated that the reversal of drug resistance by ginsenoside Rg3 is closely associated with its function of binding to cholesterol in the cell membrane and affecting the fluidity and the phase transitions of the cell membrane.

To elucidate the mode of action between ginsenoside and cholesterol, we firstly selected a fluorescent cholesterol analog Topfluor-Chol to investigate its binding capacity with ginsenoside (Figure 4H). In accordance with the potency of saponin's capacity to disrupt cell membranes, digitonin (Dig) and glycoside (GCS) were used as positive and negative controls, respectively. In an aqueous environment, a notable increase in Topfluor-Chol fluorescence intensity was observed as the Rg3 concentration increased, surpassing that of the positive control drug (Dig). Studies have shown that the enhanced emission intensity at 396 nm suggests that the aggregates of Topfluor-Chol, where self-quenching of its fluorescence occurred, dissociating upon interaction with the saponin. This interaction leads to the redistribution of Topfluor-Chol into a more hydrophobic environment. Therefore, the results demonstrated that as the concentration of Rg3 increased, the cholesterol within the solution would form aggregates with the saponins, leading to an increase in fluorescence intensity, suggesting that a combination reaction occurred between the two compounds.

Artificial microvesicles named LUVs that simulate the cell membranes were established to investigate the effect of Rg3 on cell membrane cholesterol. As is well-known, cholesterol is crucial for the structural stability of LUVs (Figure 4I, J). For LUVs constructed with cholesterol, as the concentration of the Rg3 added to the solution increased, the particle size of the LUVs grew rapidly, indicating that indicating that the LUVs were becoming increasingly unstable. In comparison, there were no

notable changes observed with LUVs without cholesterol. In addition, we observed a significant increase in cholesterol content in the supernatant of LUVs accompanied by an increase in Rg3 concentration of Rg3 concentration, indicating that Rg3 binds to cholesterol and extracts it from the cell membrane, subsequently reducing the membrane cholesterol content.

Ginsenoside Rg3 target cholesterol-enriched lipid rafts to inhibit multi-by-pass proteins function for drug resistance

Based on the binding effect of ginsenoside Rg3 on cholesterol within the cell membrane, we further studied the effects of Rg3 on membrane lipid raft and drug resistance-related proteins. Firstly, considering the co-localization of the drug-resistant membrane protein VEGFR2/FGFR1 and the lipid raft protein CAV-1 within the lipid raft area, we further investigated the effects after the treatment of Rg3(Figure 5A, B). Both proteins and lipid rafts on the cell membrane were all significantly decreased following Rg3 treatment, and extra cholesterol treatment effectively inhibited the action of Rg3. Next, the FGFR1/VEGFR2-AKT-mTOR pathway of HCC827/GR cells after Rg3 treatment was assessed using Western blot analysis (Figure 5C). The findings demonstrated that Rg3 effectively inhibited CAV-1 expression as well as both drug-resistant membrane proteins FGFR1 and VEGFR2 in HCC827/GR cells; additionally, significant suppression of the downstream AKT-mTOR signaling pathway was observed. This effect was more pronounced than that seen in single inhibitor groups and comparable to combination therapy groups. Furthermore, the effect of Rg3 on the whole pathway could be reversed by adding extra cholesterol. These results indicate that Rg3 could inhibit the expression of lipid rafts and multiple drug-resistant proteins through its interaction with membrane cholesterol, thereby blocking the activation of downstream tumor survival signaling pathways.

We then isolated lipid rafts following treatment with Rg3 (Figure 5D) and measured the cholesterol content within different layers as described earlier (Figure 5E). The results showed that, compared with the untreated group, the levels of free cholesterol and lipid raft-cholesterol in the Rg3-treatment group were both significantly decreased. Notably, Rg3 exhibited a great down-regulatory effect on cholesterol in the cholesterol-enriched lipid raft layers (layers 10-12) while other layers were not affected. As mentioned above, these cholesterol-enriched lipid raft layers are the regions where

drug-resistant proteins VEGFR2 and FGFR1 are distributed. Western blot results (Figure 5F) demonstrated that the Rg3-treatment group could effectively decrease two drug-resistant proteins at the corresponding layers. The above results indicate that cholesterol in the plasma membrane lipid raft regions, particularly those with relatively abundant cholesterol content, may serve as specific targets for Rg3. By binding cholesterol in these regions, Rg3 destabilized the lipid raft domains, ultimately leading to reduced expression of multi-drug-resistant proteins on the membrane.

Additionally, we conducted verification tests using MCF-7/PTX. In MCF-7/PTX cells, where the high expression of the ABCB1 drug-resistant protein mainly influences its drug absorption, thereby generating drug resistance. Firstly, we employed HPLC to detect PTX and flow cytometry to measure the fluorescence intensity of the ABCB1 substrate Rhodamine 123 (Figure S6), demonstrating that ginsenoside Rg3 effectively increased the intracellular PTX content, blocked its efflux, and thereby exerted the role of reversing drug resistance. Both the WB results and confocal images (Figure S7) indicated that ginsenoside Rg3 could effectively reduce the expressions of lipid raft protein CAV-1 and drug-resistant protein ABCB1, and its effects could be restored by exogenous cholesterol addition. To sum up, these results show that Rg3 can effectively impact the expressions of lipid raft proteins, thereby inhibit the activation of drug-resistant membrane proteins and downstream signaling pathways, suggesting that Rg3 might offer a potential strategy for reversing gefitinib resistance (Figure 5G).

The *in vivo* evaluation of ginsenoside Rg3 reversing gefitinib resistance

The *in vivo* antitumor experiments were performed to investigate the combination of ginsenoside Rg3 and gefitinib in inhibiting xenograft tumor growth with gefitinib resistance. After administration of different drugs for 30 days, the nude mice were sacrificed and their subcutaneous tumors were removed (Figure 6A, B). Compared to the control group, the tumor volume of gefitinib was comparable, proving the successful construction of the resistance model. The combination of ginsenoside Rg3 and gefitinib exhibited the best effects in inhibiting the growth of tumors. After calculating the tumor inhibition rates of each administration group (Figure 6C), we discovered that the tumor inhibition rate in Rg3 and gefitinib group could reach as high as 80%, while the level of the combination of one protein inhibitor and gefitinib group

was 60%, further demonstrating that the inhibitory effect on multiple membrane targets is stronger than that of a single inhibitor. Subsequently, we carried out Western blot experiments on the tumor tissues to examine the expression of related drug-resistant proteins (Figure 6D). The expressions of VEGFR2 and FGFR1 can be simultaneously inhibited by the combination treatment of Rg3 and gefitinib, where the same inhibitory effect could also be observed on the lipid raft proteins CAV-1, which was much stronger that of the combined group of inhibitors. Subsequently, we performed immunofluorescence staining on the tumor tissue sections (Figure 6E). In the tumor tissues of control and gefitinib groups, the fluorescence intensities of VEGFR2 and FGFR1 are greater and the distributions are extensive, which suggests that the abnormal expressions exist for two drug-resistant proteins. In the combination group of the inhibitors and gefitinib, the fluorescence intensities of VEGFR2 and FGFR1 were respectively attenuated and could not be simultaneously inhibited. However, under the action of Rg3 in combination with gefitinib, both fluorescence intensities were significantly decreased. Likewise, it has been demonstrated that single-target inhibitors are incapable of completely suppressing the abnormal expression of multiple proteins. Only the simultaneous suppression of multiple targets can bring about better therapeutic effects.

Furthermore, it is noteworthy that in the lung H&E staining sections of the treatment groups (Figure S8), it was observed that the single inhibitors Axitinib and PD166866, when combined with gefitinib, induced a certain degree of lung injury, characterized by obvious congestion (Figure 6F). However, the Rg3 treatment group presented no significant signs of injury, indicating that its safety profile is superior.

The cholesterol-binding ability of ginsenosides determines their reversal of drug resistance

Given the fact that the favorable reversal of drug resistance by Rg3 is attributed to its combination with membrane cholesterol, we selected 14 ginsenosides with distinct structural characteristics to investigate the correlation between their drug resistance-reversing effects and cholesterol-binding abilities. Ginsenosides can be classified into two major categories, PPD and PPT, based on their structural characteristics. Among

the 6 PPD-types ginsenosides selected (Figure 7A), Rb1, Rb2 and Rb3 showed no effects on reversing drug resistance while Rg3, Rh2 and PPD could effectively reverse gefitinib resistance. In the light of this result, we then evaluated the binding capacity of these ginsenosides with fluorescent cholesterol Topfluor-Chol (Figure 7B) as described earlier. The fluorescence intensity in Rg3, Rh2 and PPD group was significantly increased, while no change in fluorescence intensity of ginsenosides Rb1, Rb2 and Rb3 was observed, which was like that of negative control. As depicted in (Figure 7C), Filipin III enables the cholesterol in cell membranes to exhibit yellow fluorescence, and the fluorescence undergoes alterations with different ginsenosides. The ginsenosides Rb1, Rb2, and Rb3 have no substantial influence on the cholesterol in cell membranes. In comparison, fluorescence intensities after treatment with ginsenosides Rg3, Rh2, and PPD are decreased to various levels (Rg3>Rh2>PPD), which is perfectly consistent with their reversal of drug resistance effects (Rg3>Rh2>PPD). Consequently, ginsenoside Rb1, Rb2, and Rb3 which fails to bind cholesterol, lacks the ability to reverse drug resistance, whereas other ginsenosides, which possess a stronger capacity to bind cholesterol would exhibit a better efficacy in reversing drug resistance. Based on their structures, we speculate that among the PPD-type ginsenosides, the natural ginsenoside at position R2 has a sugar group, whose spatial structure would impede its ability to bind cholesterol, while at position R1, the number of sugar groups positively correlates with the ability to bind cholesterol.

Moreover, we additionally selected 8 kinds of ginsenosides of the PPT type for validation (Figure 6D). Consistent with those of PPD type ginsenosides, ginsenosides Re, R1, Rg1, and Rf, which have no ability to reverse drug resistance, could not undergo binding reactions with Topfluor-Chol, whose fluorescence intensities showed no significant changes (Figure 7E). In contrast, ginsenosides Rg2, Rh1, F1, and PPT, which possess the ability to reverse drug resistance, could bind with Topfluor-Chol to varying degrees, and the strength of their binding capacity maintained a positive correlation with their efficacy in reversing drug resistance. In PPT-type ginsenosides, likewise, the presence of a sugar group at the R2 position of the natural ginsenosides would impede its capacity to bind cholesterol due to the spatial structure, while the number of sugar groups at the R1 position is inversely proportional to the ability to bind cholesterol. Therefore, we contend that the stronger the capacity of ginsenosides to bind cholesterol, the more remarkable their effect in reversing drug resistance.

Finally, we also compared the inhibitory effects of different ginsenosides on VEGFR2 and FGFR1 proteins using ELISA kits (Figure S9), which confirmed that Rg3 was the most effective ginsenoside, which was consistent with the previous analysis results.

Discussion

Small molecule targeted drugs serve as the first-line treatment for NSCLC in clinical practice(Gridelli et al., 2011). However, as the duration of drug usage increases, resistance has emerged as a common hindrance. Currently, during EGFR-TKIs treatment, cancer cells develop resistance through both on-target and off-target mechanisms of the EGFR receptor(Cooper et al., 2022). Among these, the incidence of off-target resistance mechanisms is progressively rising in numerous clinical cases, characterized by the up-regulation of downstream signal proteins or the transformation of the phenotype after the activation of one or more by-pass signaling pathways(Mandal et al., 2024; Zhou et al., 2024). The key characteristic of resistance resulting from the activation of by-pass signaling pathways is that to successfully overcome it, dual inhibition of the driver oncogenes and by-pass pathways is necessary(Notarangelo et al., 2017; Ou et al., 2017). Although clinical trials have been carried out to combine single-target inhibitors with EGFR-TKIs for treatment, there have been no reports or effective strategies concerning the treatment resistance caused by multi-target membrane protein mutations(Fang et al., 2024). The absence of such strategies urgently calls for new treatment approaches(Xia et al., 2024). Therefore, this study established a dual-target abnormal resistance model to gefitinib in HCC827 cells and specifically explored treatment strategies and solutions for such resistance.

Then we have identified the main abnormal resistance proteins VEGFR2 and FGFR1 in the HCC827 resistant cell line and determined the downstream abnormally activated signaling pathways. To further explore the specific reasons for its resistance, we have observed that recent studies have indicated that cholesterol synthesis, uptake, or transport is disrupted in NSCLC, resulting in changes in cholesterol homeostasis(Fessler, 2023; Pan et al., 2022). It is broadly accepted that cancer cells require a considerable amount of lipids to sustain their biological membranes and maintain their uncontrolled proliferative characteristics. Lipid rafts in cell membranes

are crucial areas for the expression of protein functions, which could facilitate the growth, metastasis, and drug resistance of cancer cells(Pike, 2006; Zhao et al., 2023). The mechanism through which cholesterol confers resistance to EGFR-TKIs on NSCLC cells remains unclear. In our study, we investigated the correlation between the resistance-related proteins FGFR1, VEGFR2, and ABCB1 between lipid rafts in the HCC827/GR and MCF-7/PTX validated cell lines and discovered that after the lipid raft region expanded in response to resistance, the resistance-related proteins also migrated along with the lipid rafts and their expression increased. We maintain the belief that cholesterol-rich lipid rafts are the main triggers of by-pass resistance in NSCLC. Consequently, we chose herbal saponin compounds with the capacity to lower cholesterol for experiments on reversing drug resistance(Chen et al., 2024). As Shenyi capsule is commonly used as an adjuvant treatment for tumor drug resistance in clinical practice(Cai et al., 2021; Lu et al., 2008), ginsenoside Rg3 was selected to investigate the reverse drug resistance of different ginsenosides as we screened the reverse drug resistance. The results indicated that ginsenoside Rg3 binds to cell membrane cholesterol, reducing the cholesterol content in the lipid raft region, thereby influencing the expression of drug-resistant membrane proteins and inhibiting downstream signaling pathways to reverse drug resistance. Compared to single-target inhibitors, the effects of ginsenoside Rg3 are more significant and its safety is also an improvement on other regimens, which provided some basis for its clinical application. Meanwhile, the ability of different ginsenosides to reverse drug resistance is closely associated with their ability to bind to cell membrane cholesterol, where the stronger the binding ability, the better the reversal effect of drug resistance.

Several limitations of our study should be acknowledged. Although we used the MCF-7 cell line with resistance to paclitaxel for verification, we did not investigate the potential role in multiple protein mutations in other resistant NSCLC cells, which has certain limitations-further research in this area could help broaden the applicability of our findings. Meanwhile, the characterization of the binding mode between ginsenoside Rg3 and cholesterol is rather simplistic, and it can be further characterized by employing physical methods for a more intuitive and explicit understanding.

In summary, our research highlights a common molecular mechanism of by-pass protein-mediated gefitinib resistance in NSCLC, involving dual re-expression targets. Long-term exposure to gefitinib results in the accumulation of cholesterol in lipid rafts

in NSCLC, providing a platform for the reactivation of resistance-related proteins such as VEGFR2, FGFR1, and the AKT/mTOR signaling pathways. Significantly, this investigation demonstrates that the use of ginsenoside Rg3, by regulating the accumulation of cholesterol in lipid rafts, can inhibit the expression of resistance-related membrane proteins and the activation of downstream signaling pathways, restoring the sensitivity of tumor cells to the original drug. It proposes a safer and more effective treatment strategy for multi-target mutant EGFR-TKIs resistance, providing a theoretical basis for clinical combination strategies.

Acknowledgements

This work was supported by Programs of the National Natural Science Foundation of China [grant number 82374002, 82284066, 82204777, 82304882], Shanghai Sailing Program [grant number 21YF1422700], the fellowship of China Postdoctoral Science Foundation [grant number 2022M712155], Shuguang Program [grant number 20SG43], Program of Shanghai Academic/Technology Research Leader [grant number 22XD1423000], Shanghai Science and technology innovation project [grant number 22S21901200], the Innovation activity plan for College Students of SHUTCM [grant number 202210268191], Natural Science Foundation of Shanghai [grant number 21ZR1460800, 22ZR1459000].

Author contributions

C.H. and Y.D. provided the academic interpretation of the research work. M.J. conducted the experiments, prepared the manuscript and designed the figures. W.K.Z carried out the lipid rafts related experiments and data processing. Z.Y. and K.X.G. contributed to the *in vivo* and *in vitro* experiments. Y.N.R. and M.F.L. accomplished the review of the literature and the inspection of the manuscript. D.G. is primarily responsible for refining the textual content of the article. Furthermore, corresponding authors Y.D. and T.Z. funded this project and revised the manuscript. Y.D. and C.H. were also responsible for handling the revisions and resubmission of revised manuscripts. All authors read and approved the final manuscript.

Competing interests

The authors declare no competing interests.

References:

Arabi, S.M., Shahraki-Jazinaki, M., Abadi, M.N., Bahrami, L.S., Chambari, M., Bahari, H., Sahebkar, A., 2024, The Effect of Ginseng Supplementation on Lipid Profile: GRADE-assessed Systematic Review and Dose-response Meta-analysis of Randomized Controlled Trials. CURR PHARM DESIGN 30, 2047-2058.

Cai, Z., Teng, Y., Chen, Y., 2021, The Effect of Shenyi Capsule on Non-Small-Cell Lung Cancer Combined with Chemotherapy from the Yin-Yang Perspective. EVID-BASED COMPL ALT 2021, 1653750.

Chen, L., Chen, W.D., Xu, Y.X., Ren, Y.Y., Zheng, C., Lin, Y.Y., Zhou, J.L., 2024, Strategies for enhancing non-small cell lung cancer treatment: Integrating Chinese herbal medicines with epidermal growth factor receptor-tyrosine kinase inhibitors therapy. EUR J PHARMACOL 980, 176871.

Cho, B.C., Kim, D.W., Spira, A.I., Gomez, J.E., Haura, E.B., Kim, S.W., Sanborn, R.E., Cho, E.K., Lee, K.H., Minchom, A., Lee, J.S., Han, J.Y., Nagasaka, M., Sabari, J.K., Ou, S.I., Lorenzini, P., Bauml, J.M., Curtin, J.C., Roshak, A., Gao, G., Xie, J., Thayu, M., Knoblauch, R.E., Park, K., 2023, Amivantamab plus lazertinib in osimertinib-relapsed EGFR-mutant advanced non-small cell lung cancer: a phase 1 trial. NAT MED 29, 2577-2585.

Clark, S.B., Alsubait, S., 2024, Non-Small Cell Lung Cancer.

Cooper, A.J., Sequist, L.V., Lin, J.J., 2022, Third-generation EGFR and ALK inhibitors: mechanisms of resistance and management. NAT REV CLIN ONCOL 19, 499-514.

Denis, M.G., Vallee, A., Theoleyre, S., 2015, EGFR T790M resistance mutation in non small-cell lung carcinoma. CLIN CHIM ACTA 444, 81-85.

Fang, W., Zhao, Y., Luo, Y., Yang, R., Huang, Y., He, Z., Zhao, H., Li, M., Li, K., Song, Q., Du X, Sun, Y., Li, W., Xu, F., Wang, Z., Yang, K., Fan, Y., Liu, B., Zhao, H., Hu, Y., Jia, L., Xu, S., Yi, T., Lv, D., Lan, H., Li, M., Liang, W., Wang, Y., Yang, H., Jia, Y., Chen, Y., Lu, J., Feng, J., Liu, C., Zhou, M., Zhou, J., Liu, X., Zhou, N., He, M., Dong, X., Chen, H., Chen, Y., Su, H., Li, X., Zhang, Z., Yang, L., Cheng, Y., Chen, L., Hou, X., Zhang, Y., Guo, J., Wang, Z., Lu, H., Wu, D., Feng, W., Li, W., Huang, J., Wang, Y., Song, X., Peng, J., Liu, L., Guo, Y., Li, W., Lu, D., Hu, M., Wang, Z.M., Li, B., Xia, M., Zhang, L., 2024, Ivonescimab Plus Chemotherapy in Non-Small Cell Lung Cancer With EGFR Variant: A Randomized Clinical Trial. JAMA-J AM MED ASSOC 332, 561-570.

Fenyvesi, F., Fenyvesi, E., Szente, L., Goda, K., Bacso, Z., Bacskay, I., Varadi, J., Kiss, T., Molnar, E., Janaky, T., Szabo, G.J., Vecsernyes, M., 2008, P-glycoprotein inhibition by membrane cholesterol modulation. EUR J PHARM SCI 34, 236-242.

Fessler, M.B., 2023, We need to talk about lung cancer's cholesterol-hoarding problem. CELL STEM CELL 30, 745-747.

Gajate, C., Mollinedo, F., 2021, Lipid Raft Isolation by Sucrose Gradient Centrifugation and Visualization of Raft-Located Proteins by Fluorescence Microscopy: The Use of Combined Techniques to Assess Fas/CD95 Location in Rafts During Apoptosis Triggering. Methods Mol Biol 2187, 147-186.

Ganti, A.K., Klein, A.B., Cotarla, I., Seal, B., Chou, E., 2021, Update of Incidence, Prevalence, Survival, and Initial Treatment in Patients With Non-Small Cell Lung Cancer in the US. JAMA ONCOL 7, 1824-1832.

Garza-Miyazato, D., Hanashima, S., Umegawa, Y., Murata, M., Kinoshita, M., Matsumori, N., Greimel, P., 2024, Mode of molecular interaction of triterpenoid saponin ginsenoside Rh2 with membrane lipids in liquid-disordered phases. BBA-BIOMEMBRANES 1866, 184366.

Gridelli, C., De Marinis, F., Di Maio, M., Cortinovis, D., Cappuzzo, F., Mok, T., 2011, Gefitinib as first-line treatment for patients with advanced non-small-cell lung cancer with activating epidermal growth factor receptor mutation: Review of the evidence. LUNG CANCER 71, 249-257.

Gu, L., Pillay, R.P., Aronson, R., Kaur, M., 2024, Cholesteryl ester transfer protein knock-down in conjunction with a cholesterol-depleting agent decreases tamoxifen resistance in breast cancer cells. IUBMB LIFE 76, 712-730.

Gupta, V.K., Sharma, N.S., Kesh, K., Dauer, P., Nomura, A., Giri, B., Dudeja, V., Banerjee, S., Bhattacharya, S., Saluja, A., Banerjee, S., 2018, Metastasis and chemoresistance in CD133 expressing pancreatic cancer cells are dependent on their lipid raft integrity. CANCER LETT 439, 101-112.

Huang, B., Song, B.L., Xu, C., 2020, Cholesterol metabolism in cancer: mechanisms and therapeutic opportunities. NAT METAB 2, 132-141.

Husain, H., Scur, M., Murtuza, A., Bui, N., Woodward, B., Kurzrock, R., 2017, Strategies to Overcome Bypass Mechanisms Mediating Clinical Resistance to EGFR Tyrosine Kinase Inhibition in Lung Cancer. MOL CANCER THER 16, 265-272.

Isik, O.A., Cizmecioglu, O., 2023, Rafting on the Plasma Membrane: Lipid Rafts in Signaling and Disease. ADV EXP MED BIOL 1436, 87-108.

Kuzu, O.F., Noory, M.A., Robertson, G.P., 2016, The Role of Cholesterol in Cancer. CANCER RES 76, 2063-2070.

Kwon, H.Y., Kim, E.H., Kim, S.W., Kim, S.N., Park, J.D., Rhee, D.K., 2008, Selective toxicity of ginsenoside Rg3 on multidrug resistant cells by membrane fluidity modulation. ARCH PHARM RES 31, 171-177.

Laurens, W.E., Vanrenterghem, Y.F., Steels, P.S., Van Damme, B.J., 1994, A new single nephron model of focal and segmental glomerulosclerosis in the Munich-Wistar rat. KIDNEY INT 45, 143-149.

Liu, G., Chen, T., Ding, Z., Wang, Y., Wei, Y., Wei, X., 2021, Inhibition of FGF-FGFR and VEGF-VEGFR signalling in cancer treatment. CELL PROLIFERAT 54, e13009.

Liu, Q., Yu, S., Zhao, W., Qin, S., Chu, Q., Wu, K., 2018, EGFR-TKIs resistance via EGFR-independent signaling pathways. MOL CANCER 17, 53.

Liu, Y., Yang, G., Bu, X., Liu, G., Ding, J., Li, P., Jia, W., 2011, Cell-type-specific regulation of raft-associated Akt signaling. CELL DEATH DIS 2, e145.

Lorent, J.H., Leonard, C., Abouzi, M., Akabi, F., Quetin-Leclercq, J., Mingeot-Leclercq, M.P., 2016, alpha-Hederin Induces Apoptosis, Membrane Permeabilization and Morphologic Changes in Two Cancer Cell Lines Through a Cholesterol-Dependent Mechanism. PLANTA MED 82, 1532-1539.

Lu, P., Su, W., Miao, Z.H., Niu, H.R., Liu, J., Hua, Q.L., 2008, Effect and mechanism of ginsenoside Rg3 on postoperative life span of patients with non-small cell lung cancer. CHIN J INTEGR MED 14, 33-36.

Lucero, H.A., Robbins, P.W., 2004, Lipid rafts-protein association and the regulation of protein activity. ARCH BIOCHEM BIOPHYS 426, 208-224.

Lv, Y., Zhang, C.D., Wang, Y.L., Zhou, D.M., Zhu, M.Y., Hao, X.Q., Wang, J.H., Gu, W.Z., Shen, H.Q., Lou, J.G., Wu, B.Q., Chen, P.C., Zhao, Z.Y., 2021, Synergism of rMV-Hu191 with cisplatin to treat gastric cancer by acid sphingomyelinase-mediated apoptosis requiring integrity of lipid raft

microdomains. GASTRIC CANCER 24, 1293-1306.
Malabed, R., Hanashima, S., Murata, M., Sakurai, K., 2017, Sterol-recognition ability and membrane-disrupting activity of Ornithogalum saponin OSW-1 and usual 3-O-glycosyl saponins. BBA-BIOMEMBRANES 1859, 2516-2525.
Mandal, J., Jones, T.N., Liberto, J.M., Gaillard, S., Wang, T.L., Shih, I.M., 2024, Dual Inhibition of SYK and EGFR Overcomes Chemoresistance by Inhibiting CDC6 and Blocking DNA Replication. CANCER RES 84, 3881-3893.
Notarangelo, T., Sisinni, L., Condelli, V., Landriscina, M., 2017, Dual EGFR and BRAF blockade overcomes resistance to vemurafenib in BRAF mutated thyroid carcinoma cells. CANCER CELL INT 17, 86.
Ou, S.I., Horn, L., Cruz, M., Vafai, D., Lovly, C.M., Spradlin, A., Williamson, M.J., Dagogo-Jack, I., Johnson, A., Miller, V.A., Gadgeel, S., Ali, S.M., Schrock, A.B., 2017, Emergence of FGFR3-TACC3 fusions as a potential by-pass resistance mechanism to EGFR tyrosine kinase inhibitors in EGFR mutated NSCLC patients. LUNG CANCER 111, 61-64.
Pan, Z., Wang, K., Wang, X., Jia, Z., Yang, Y., Duan, Y., Huang, L., Wu, Z.X., Zhang, J.Y., Ding, X., 2022, Cholesterol promotes EGFR-TKIs resistance in NSCLC by inducing EGFR/Src/Erk/SP1 signaling-mediated ERRalpha re-expression. MOL CANCER 21, 77.
Pan, Z., Wang, K., Wang, X., Jia, Z., Yang, Y., Duan, Y., Huang, L., Wu, Z.X., Zhang, J.Y., Ding, X., 2022, Cholesterol promotes EGFR-TKIs resistance in NSCLC by inducing EGFR/Src/Erk/SP1 signaling-mediated ERRalpha re-expression. MOL CANCER 21, 77.
Park, E.K., Lee, E.J., Lee, S.H., Koo, K.H., Sung, J.Y., Hwang, E.H., Park, J.H., Kim, C.W., Jeong, K.C., Park, B.K., Kim, Y.N., 2010, Induction of apoptosis by the ginsenoside Rh2 by internalization of lipid rafts and caveolae and inactivation of Akt. BRIT J PHARMACOL 160, 1212-1223.
Pike, L.J., 2006, Rafts defined: a report on the Keystone Symposium on Lipid Rafts and Cell Function. J LIPID RES 47, 1597-1598.
Pike, L.J., 2006, Rafts defined: a report on the Keystone Symposium on Lipid Rafts and Cell Function. J LIPID RES 47, 1597-1598.
Qiu, J., Li, W., Feng, S.H., Wang, M., He, Z.Y., 2014, Ginsenoside Rh2 promotes nonamyloidgenic cleavage of amyloid precursor protein via a cholesterol-dependent pathway. GENET MOL RES 13, 3586-3598.
Qiu, R., Zhang, J., Ge, C., Zhong, Y., Liu, S., Li, Q., Zou, J., Fan, H., Li, Y., 2022, Ginsenosides Rg1 and CK Control Temozolomide Resistance in Glioblastoma Cells by Modulating Cholesterol Efflux and Lipid Raft Distribution. EVID-BASED COMPL ALT 2022, 1897508.
Rabani, V., Davani, S., Gambert-Nicot, S., Meneveau, N., Montange, D., 2016, Comparative lipidomics and proteomics analysis of platelet lipid rafts using different detergents. PLATELETS 27, 634-641.
Riely, G.J., Wood, D.E., Ettinger, D.S., Aisner, D.L., Akerley, W., Bauman, J.R., Bharat, A., Bruno, D.S., Chang, J.Y., Chirieac, L.R., DeCamp, M., Desai, A.P., Dilling, T.J., Dowell, J., Durm, G.A., Gettinger, S., Grotz, T.E., Gubens, M.A., Juloori, A., Lackner, R.P., Lanuti, M., Lin, J., Loo, B.W., Lovly, C.M., Maldonado, F., Massarelli, E., Morgensztern, D., Mullikin, T.C., Ng, T., Owen, D., Owen, D.H., Patel, S.P., Patil, T., Polanco, P.M., Riess, J., Shapiro, T.A., Singh, A.P., Stevenson, J., Tam, A., Tanvetyanon, T., Yanagawa, J., Yang, S.C., Yau, E., Gregory, K.M., Hang, L., 2024, Non-Small Cell Lung Cancer, Version 4.2024, NCCN Clinical Practice Guidelines in Oncology. J NATL COMPR CANC NE 22, 249-274.

Ruzzi, F., Cappello, C., Semprini, M.S., Scalambra, L., Angelicola, S., Pittino, O.M., Landuzzi, L., Palladini, A., Nanni, P., Lollini, P.L., 2024, Lipid rafts, caveolae, and epidermal growth factor receptor family: friends or foes? CELL COMMUN SIGNAL 22, 489.

Soria, J.C., Ohe, Y., Vansteenkiste, J., Reungwetwattana, T., Chewaskulyong, B., Lee, K.H., Dechaphunkul, A., Imamura, F., Nogami, N., Kurata, T., Okamoto, I., Zhou, C., Cho, B.C., Cheng, Y., Cho, E.K., Voon, P.J., Planchard, D., Su, W.C., Gray, J.E., Lee, S.M., Hodge, R., Marotti, M., Rukazenkov, Y., Ramalingam, S.S., 2018, Osimertinib in Untreated EGFR-Mutated Advanced Non-Small-Cell Lung Cancer. NEW ENGL J MED 378, 113-125.

Wang, C., Zhang, Y., Zhang, T., Xu, J., Yan, S., Liang, B., Xing, D., 2023, Epidermal growth factor receptor dual-target inhibitors as a novel therapy for cancer: A review. INT J BIOL MACROMOL 253, 127440.

Westover, D., Zugazagoitia, J., Cho, B.C., Lovly, C.M., Paz-Ares, L., 2018, Mechanisms of acquired resistance to first- and second-generation EGFR tyrosine kinase inhibitors. ANN ONCOL 29, i10-i19.

Wu, S.C., Lo, Y.M., Lee, J.H., Chen, C.Y., Chen, T.W., Liu, H.W., Lian, W.N., Hua, K., Liao, C.C., Lin, W.J., Yang, C.Y., Tung, C.Y., Lin, C.H., 2022, Stomatin modulates adipogenesis through the ERK pathway and regulates fatty acid uptake and lipid droplet growth. NAT COMMUN 13, 4174.

Wu, S.G., Shih, J.Y., 2018, Management of acquired resistance to EGFR TKI-targeted therapy in advanced non-small cell lung cancer. MOL CANCER 17, 38.

Xia, Y., Wang, K., Zhao, J., Arter, Z., Zhang, Y., Zhou, J., Lu, Y., Zeng, L., Du R, Owens, J.A., Elamin, Y.Y., Gay, C.M., Skoulidis, F., Tsao, A.S., Lu, C., Cascone, T., Gibbons, D.L., Zhang, J., Chen, O., Mok, K.K., Nagasaka, M., Li, W., Heymach, J.V., Ignatius, O.S., Li, M., Le X, 2024, Receptor tyrosine kinase fusion-mediated resistance to EGFR-TKI in EGFR-mutant NSCLC: a multi-center analysis and literature review. J THORAC ONCOL.

Yun, U.J., Lee, J.H., Koo, K.H., Ye, S.K., Kim, S.Y., Lee, C.H., Kim, Y.N., 2013, Lipid raft modulation by Rp1 reverses multidrug resistance via inactivating MDR-1 and Src inhibition. BIOCHEM PHARMACOL 85, 1441-1453.

Zhang, X., Tan, Y., Li, T., Tan, D., Fu, B., Yang, M., Chen, Y., Cao, M., Xuan, C., Du Q, Hu, R., Wang, Q., 2024, Intercellular adhesion molecule-1 suppresses TMZ chemosensitivity in acquired TMZ-resistant gliomas by increasing assembly of ABCB1 on the membrane. DRUG RESIST UPDATE 76, 101112.

Zhao, X., Guo, B., Sun, W., Yu, J., Cui, L., 2023, Targeting Squalene Epoxidase Confers Metabolic Vulnerability and Overcomes Chemoresistance in HNSCC. ADV SCI 10, e2206878.

Zhou, F., Guo, H., Xia, Y., Le X, Tan, D., Ramalingam, S.S., Zhou, C., 2024, The changing treatment landscape of EGFR-mutant non-small-cell lung cancer. NAT REV CLIN ONCOL.

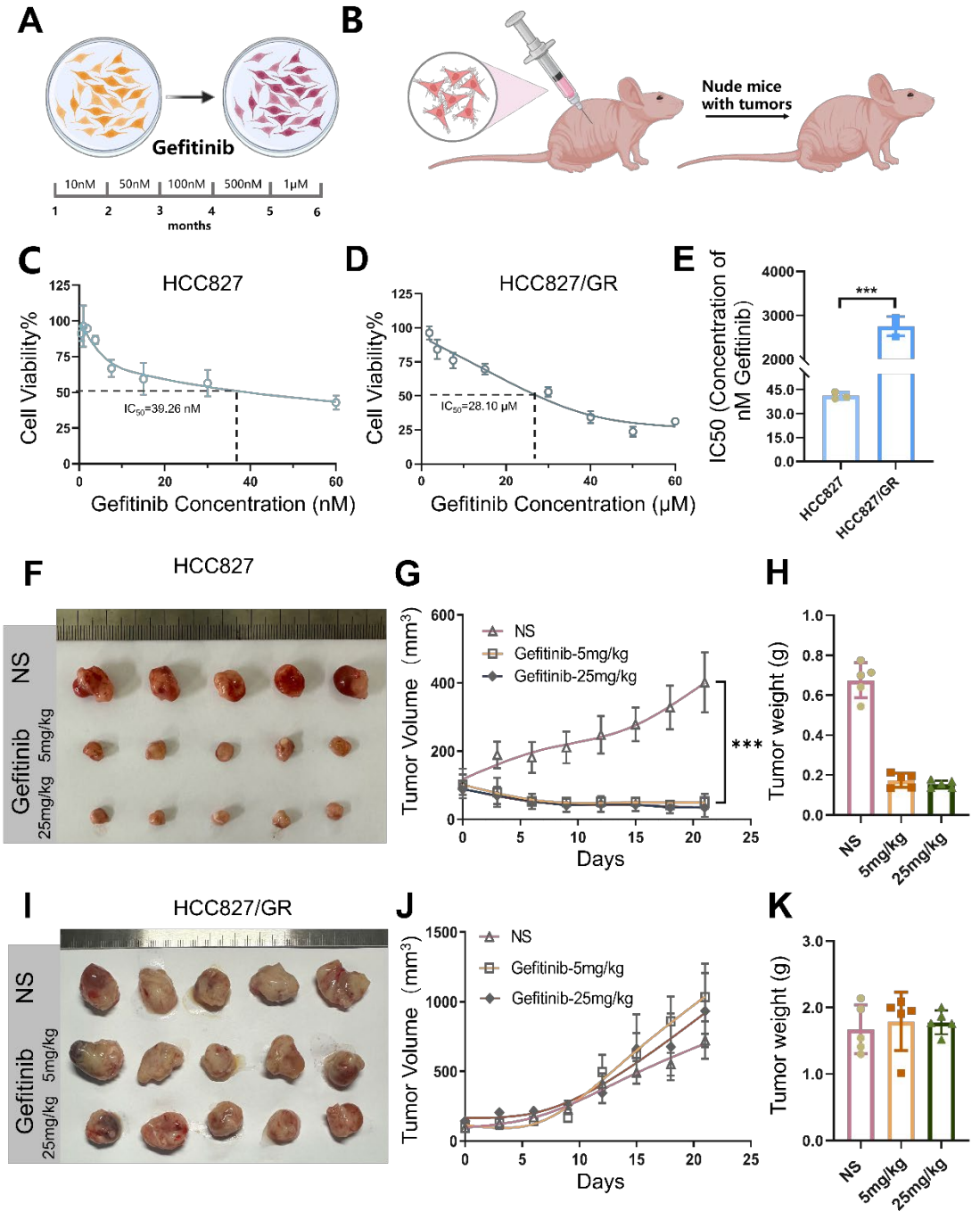

Fig.1 Establishment of the gefitinib-resistant tumor models. (**A**) HCC827 cells were exposed to gefitinib for six months to generate gefitinib-resistant HCC827/GR cells. (**B**) Subcutaneous injection of HCC827 and HCC827/GR cells were performed to construct the tumor-bear model in nude mice. (**C-E**) CCK-8 assay was used to detect the IC_{50} values of the drug-resistant cells treated with gefitinib in HCC827 and HCC827/GR cells. In the HCC827 and HCC827/GR tumor models, when the tumor reached 100 mm^3, NS groups were treated with PBS and gefitinib groups were treated with gefitinib high-dose (25mg/kg) and low-dose (5mg/kg) by intragastric administration. After 21 days of administration, the mice were sacrificed, the tumors were removed for photography (**F, I**), the tumor volume was recorded every three days (**G, J**), and finally the tumors were weighed to record the inhibition rate (**H, K**). All the results

are shown as mean ± SD （n = 5, *$p < 0.05$, **$p < 0.01$,***$p < 0.001$）.

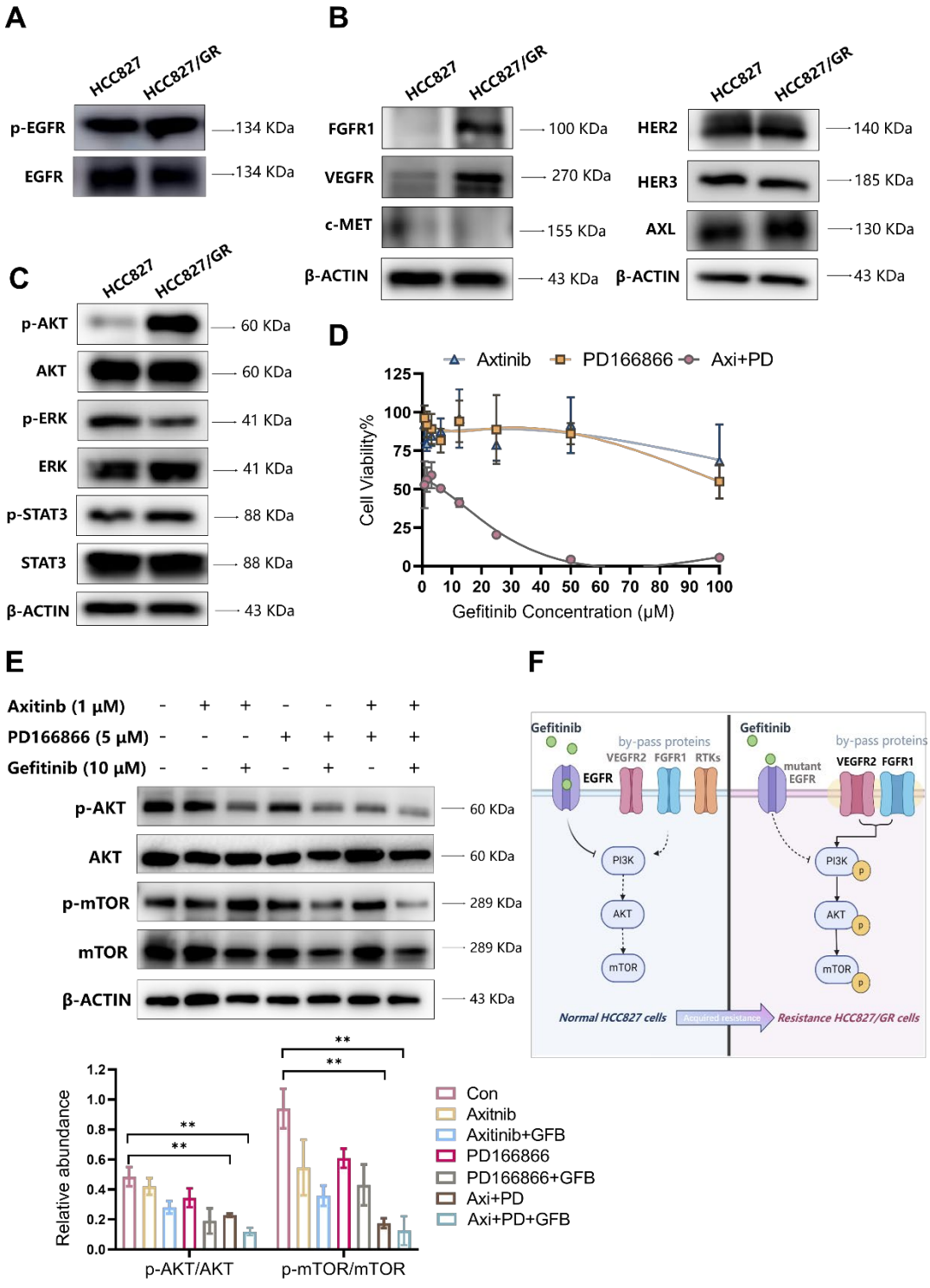

Fig.2 The mechanism of mutations in multi-target membrane proteins subsequent to gefitinib resistance. (**A**) A comparison of p-EGFR in HCC827 and drug-resistant HCC827/GR cell. (**B**) Detection of the protein expression of six by-pass membrane proteins. (**C**) Examination of the

efficacy of single inhibitors, namely VEGFR2 inhibitor (axitinib), FGFR1 inhibitor (PD166866), and their combination therapy in reversing drug resistance. (**D**) Examination of the expression profiles of the three downstream classical signaling pathways. (**E**) Western blot results showed the downstream pathway proteins expression after treatment with axitinib, PD166866 and both in combination with gefitinib. (**F**) The key associated proteins and signaling pathways implicated in the development of resistance in HCC827/GR.

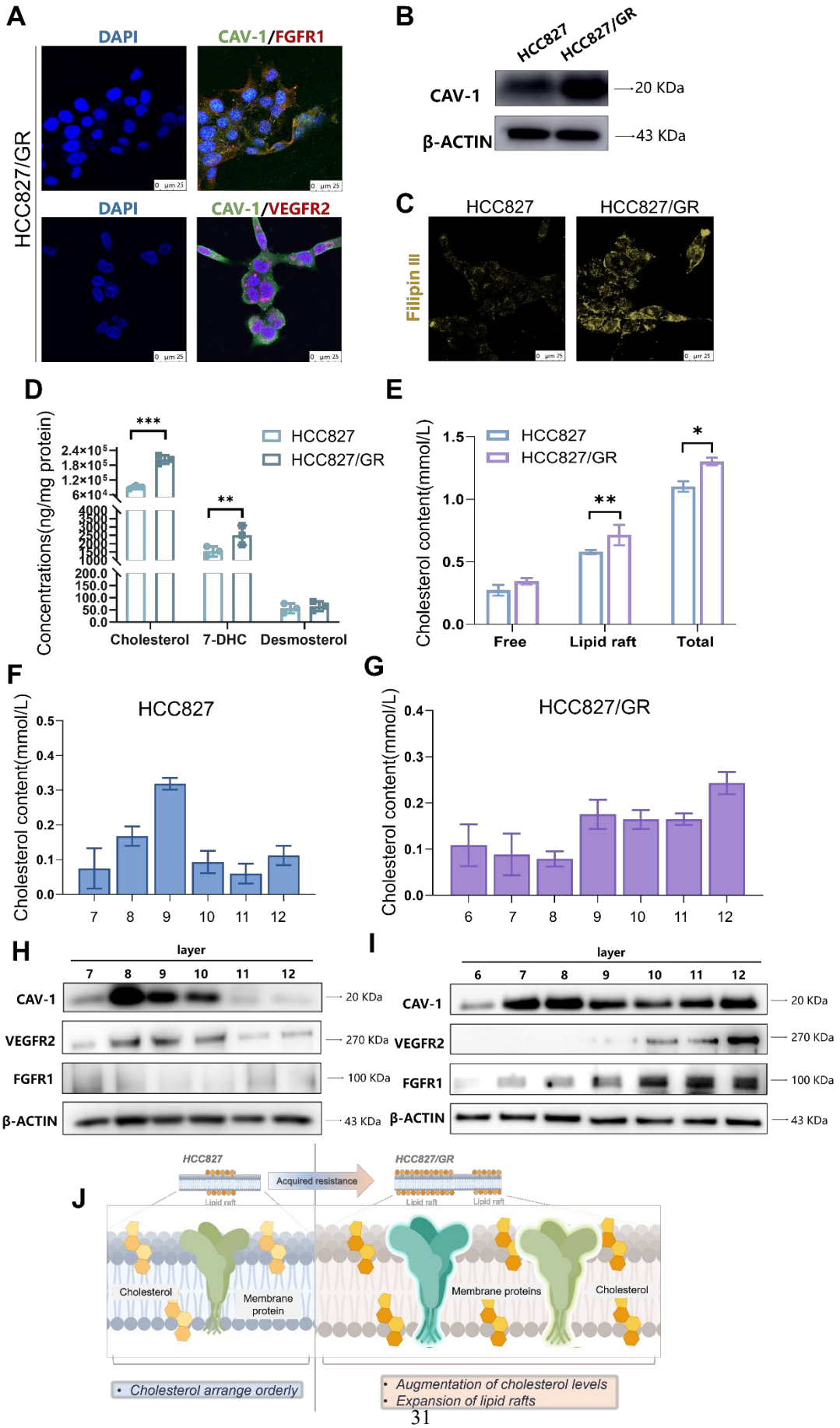
A
DAPI
CAV-1/FGFR1
DAPI
CAV-1/VEGFR2
HCC827/GR
B
HCC827
HCC827/GR
CAV-1
20 KDa
β-ACTIN
43 KDa
C
HCC827
HCC827/GR
Filipin III
D
Concentrations(ng/mg protein)
HCC827
HCC827/GR
Cholesterol
7-DHC
Desmosterol
E
Cholesterol content(mmol/L)
HCC827
HCC827/GR
Free
Lipid raft
Total
F
HCC827
Cholesterol content(mmol/L)
G
HCC827/GR
Cholesterol content(mmol/L)
H
layer
CAV-1
VEGFR2
FGFR1
β-ACTIN
20 KDa
270 KDa
100 KDa
43 KDa
I
layer
CAV-1
VEGFR2
FGFR1
β-ACTIN
20 KDa
270 KDa
100 KDa
43 KDa
J
HCC827
Acquired resistance
HCC827/GR
Lipid raft
Cholesterol
Membrane protein
Membrane proteins
Cholesterol
• Cholesterol arrange orderly
• Augmentation of cholesterol levels
• Expansion of lipid rafts

Fig.3 The accumulation of cholesterol within lipid rafts leads to the emergence of abnormal mutations in membrane proteins associated with drug-resistance. **(A)** CAV-1 serves as a biomarker for lipid rafts. The HCC827/GR were immunoassayed for VEGFR2, FGFR1 (red), CAV-1 (green), and nucleus (DAPI, blue). **(B)** The discrepant expression of CAV-1 in HCC827 and HCC827/GR cells. **(C)** Cells were incubated with Filipin III for 1 h. Confocal images to determine the presence of cell mambrane cholesterol in yellow and the fluorescence intensity was analyzed. **(D)** The total amount of cholesterol in the cells was detected by LC-MS to compare the discrepancy between the sensitive strains and drug-resistant strains. **(E)** Density gradient centrifugation for the isolation of lipid rafts. The contents of free cholesterol, lipid raft cholesterol and total cholesterol at various layers. **(F, G)** The contents of lipid raft cholesterol in HCC827 and HCC827/GR cells. **(H, I)** The distribution of CAV-1 and VEGFR2, FGFR1 at different layers in HCC827 and HCC827/GR cells. **(J)** A diagram showing the accumulation of cholesterol in lipid rafts of the cell membrane and the increase in its concentration after acquired drug resistance, leading to the expansion of functional domains.

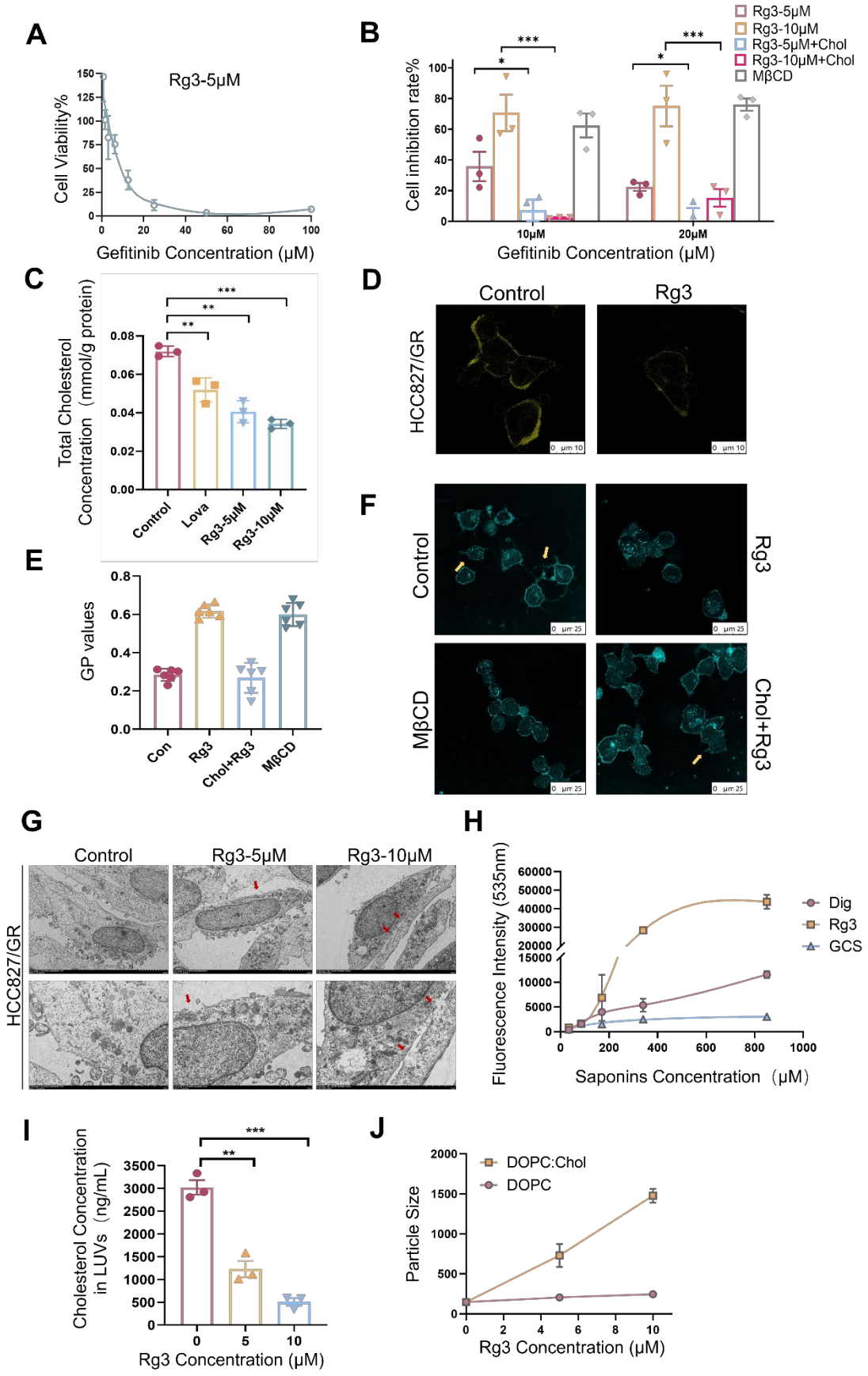

Fig.4 Ginsenoside Rg3 combines with membrane cholesterol to reverse drug resistance. **(A)**

The CCK-8 assay was deployed to examine the reversing effect on drug resistance under the action of 5 μM ginsenoside Rg3. (**B**) The HCC827/GR cells were treated with gefitinib + 5 μM Ginsenoside Rg3, gefitinib + 10 μM Ginsenoside Rg3, gefitinib + 5 μM Ginsenoside Rg3 + 5 μM cholesterol and gefitinib + 10 μM Ginsenoside Rg3 + 5 μM cholesterol for 48 h. Then the cell viability was measured by CCK-8 assay. (**C**) HCC827/GR were treated with 2 μM Lovastain (lova), 5 μM Ginsenoside Rg3 and 10 μM Ginsenoside Rg3 for 24 h, then cholesterol level in the indicated cells were determined via a total cholesterol assay. (**D**) Confocal microscopy was used to observe the changes in the cell membrane cholesterol after the treatment with ginsenoside Rg3 as detected by the Filipin III assay. (**E, F**) HCC827/GR cells were treated with 5 μM Rg3, 5 μM Rg3 + 5 μM cholesterol and 5mM MβCD, then incubated with Luardan and the distribution of GP values in a living cell. (**G**)The destruction of cell membrane by ginsenoside Rg3 was observed by transmission electron microscopy in indicated cells. (**H**) Fluorescence intensities of TopFluor® Cholesterol at different saponin concentrations. Digitonin was the positive control and GCS was the negative control. (**I, J**) Simulated particle size changes of LUVs treated with different concentrations of Rg3 and the remaining cholesterol concentration was tested by LC-MS.

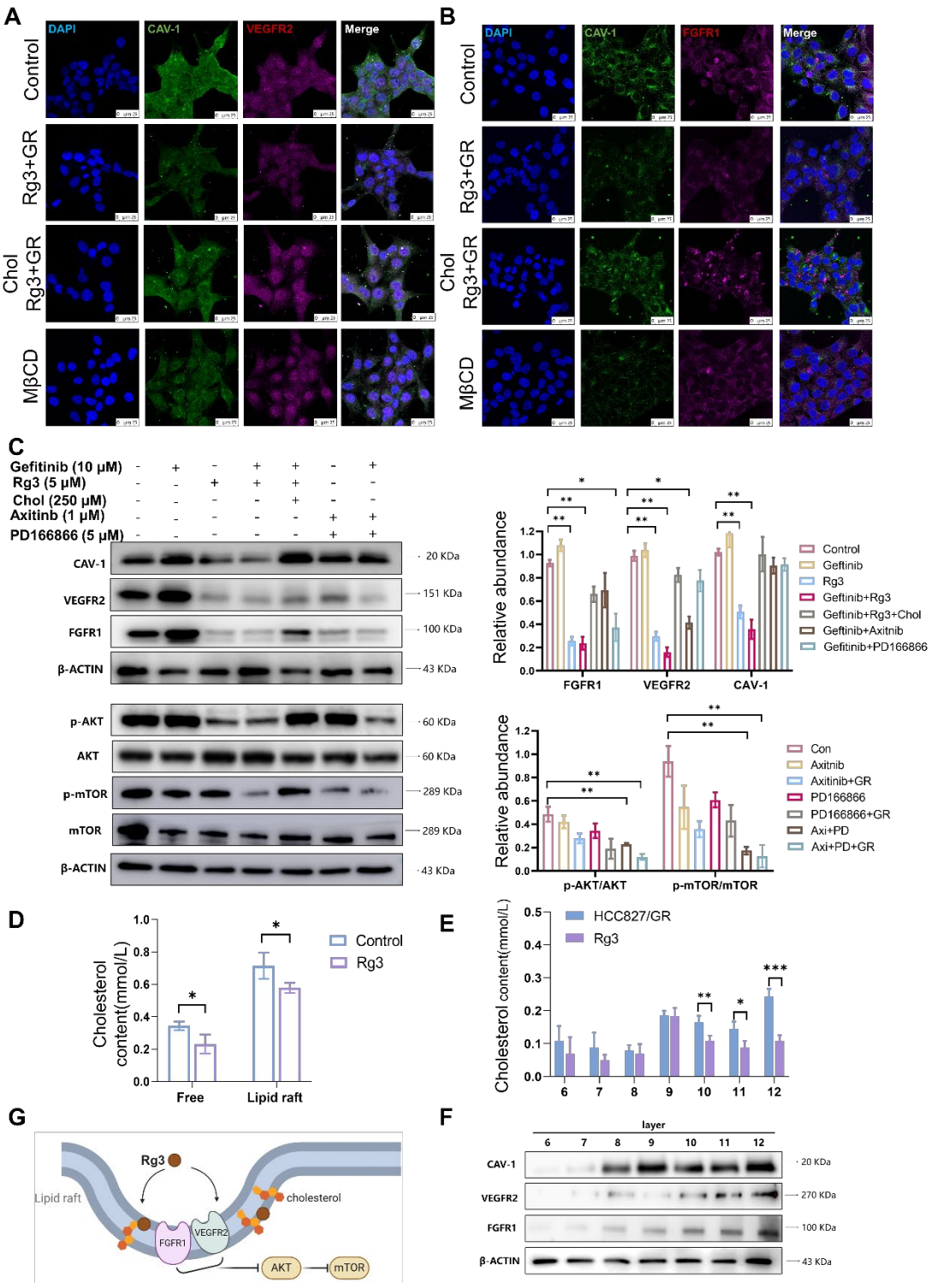

Fig.5 Ginsenoside Rg3 modulates the lipid rafts function to inhibit dual-by-pass proteins mediated downstream signaling activation. (**A**) The mechanism of Ginsenoside Rg3 binds to lipid raft cholesterol and inhibits the expression of membrane proteins. (**B**) After treatment with ginsenoside Rg3 (Rg3, 5 μM), the contents of free and lipid raft cholesterol. (**C**) Western blot was employed to detect the expression of lipid raft protein CAV-1 and drug resistance-related proteins VEGFR2 and FGFR1 at different levels after the effect of ginsenoside Rg3 and semi-quantitative analysis chart. **(D)**The content of cholesterol in the lipid raft layers after the

treatment of ginsenoside Rg3. (**E**) The cholesterol content at different levels after the treatment of Rg3. (**F**) Western Blot assay was used to detect the expression of FGFR1 and VEGFR2 proteins after Rg3 treated at different levels. (**G**) The mechanism of Rg3 based on membrane cholesterol- lipid rafts- membrane proteins axis.

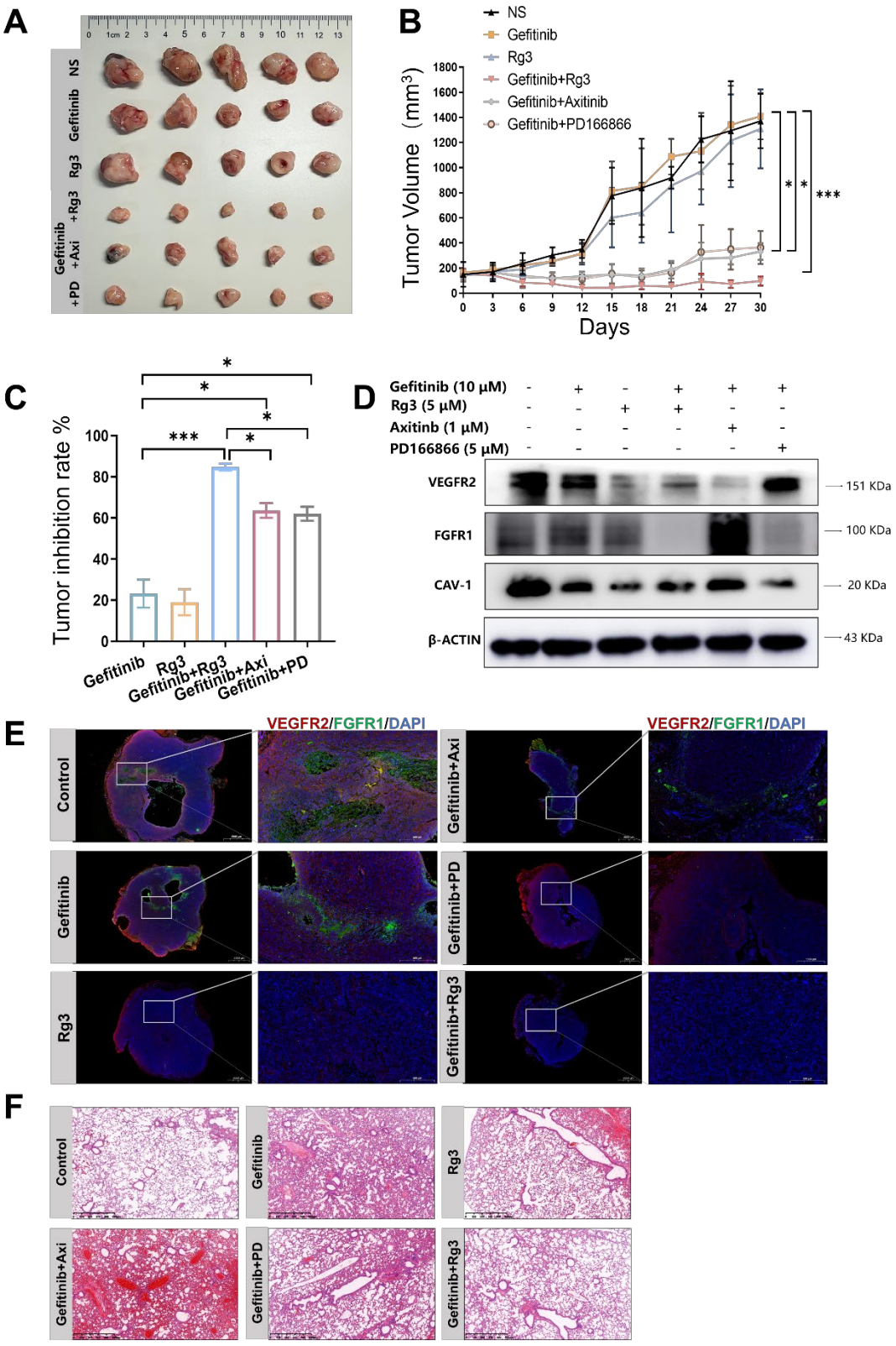

Fig.6 Evaluation of the *in vivo* pharmacodynamic effect of reversing gefitinib resistance by ginsenoside Rg3. (**A**) In subcutaneous xenograft mouse models, HCC827/GR cells were implanted into the right flanks of BALB/c nude mice, followed by treatment with NS, Gefitinib (2.5 mg/kg), Rg3 (20 mg/kg), Gefitinib+Rg3, Gefitinib+Axitinib (0.5 mg/kg) and

Gefitinib+PD166866 (0.5 mg/kg) when the tumor reached a volume of approximately 150 mm^3 in size, tumor growth was assessed every 3 days. Following 30 days of treatment, the mice were euthanized. (**B, C**) Tumor appearance, tumor growth and tumor inhibitory levels are shown. (**D**) Western blot assay measured VEGFR2, FGFR1 and CAV-1 proteins level in tumor tissues. **(E)** Immunofluorescence staining of tumor tissues. Red fluorescence represents VEGFR2, green fluorescence represents FGFR1 and blue fluorescence represents CAV-1. **(F)** H&E staining sections of lung tissues.

A

	Propanaxandiol	Total Glycosyl	C-3	C-20		Reversal multiple
			R1	R2	R3	
Natural Ginseno side	Rb1	4	-glc(2-1)glc	-Oglc(6-1)glc	-CH3	/
	Rb2	4	-glc(2-1)glc	-Oglc(6-1)arap	-CH3	/
	Rb3	4	-glc(2-1)glc	-Oglc(6-1)xyl	-CH3	/
Rare Ginseno side	20-(S)Rg3	2	-glc(2-1)glc	-OH	-CH3	86.3
	20-(S)Rh2	1	-glc	-OH	-CH3	41.5
	20-(S)PPD	0	-H	-OH	-CH3	19.0

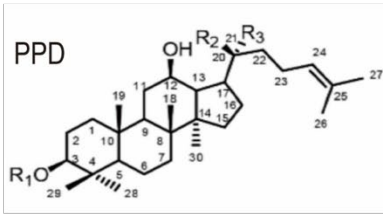

B

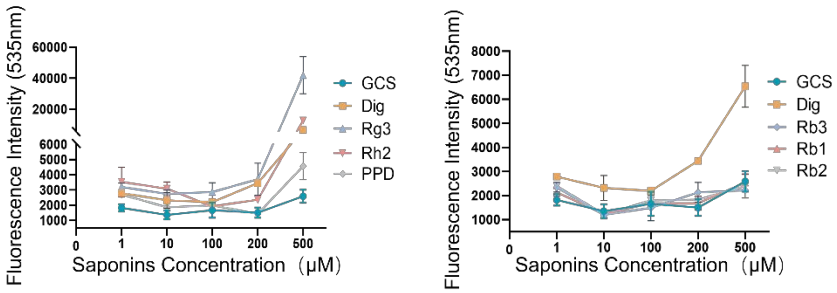

C

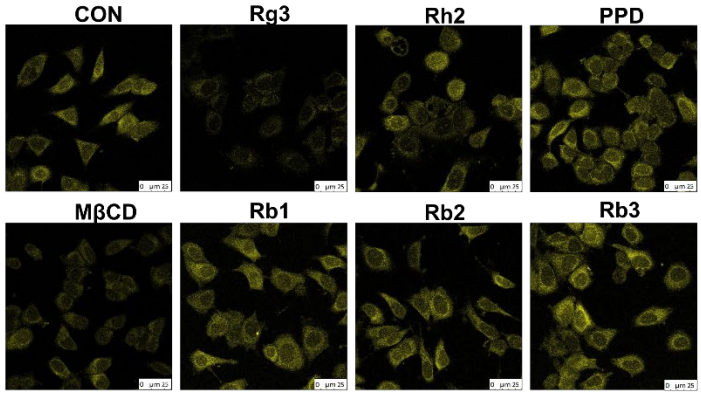

D

	Propanaxtriol	Total Glycosyl	C-6	C-20		Reversal multiple
			R1	R2	R3	
Natural Ginseno side	Re	3	-glc(2-1)rha	-Oglc	-CH3	/
	R1	3	-glc(2-1)xyl	-Oglc	-CH3	/
	Rg1	2	-glc	-Oglc	-CH3	/
	Rf	2	-glc(2-1)glc	-OH	-CH3	/
Rare Ginseno side	20-(S)Rg2	2	-glc(2-1)rha	-OH	-CH3	9.5
	20-(S)Rh1	1	-glc	-OH	-CH3	12.9
	F1	1	-H	-Oglc	-CH3	26.6
	20-(S)PPT	0	-H	-OH	-CH3	27.5

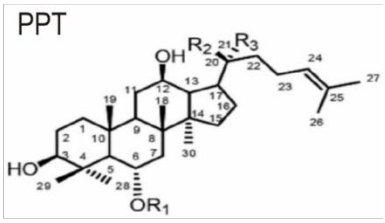

E

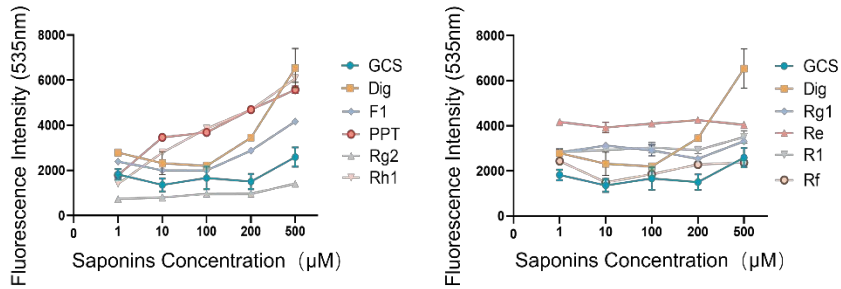

Fig.7 The effect of different ginsenosides on drug resistance reversal and cholesterol binding ability. (**A-B**) In HCC827/GR cells, 14 kinds of ginsenosides reversed drug resistance and reversal times. And the structure of PPT and PPD ginsenosides. (**C**) The binding effect of 14 ginsenosides with fluorescent cholesterol. Dig was used as the positive control, and GCS was

used as the negative control. (**D**) Filipin III staining was used to observe the effects of PPD type 6 ginsenosides on cell membrane cholesterol content. MβCD was treated as the positive control.